HHS Public Access

Author manuscript

Plant J. Author manuscript; available in PMC 2015 May 01.

Published in final edited form as:

Plant J. 2014 May ; 78(3): 452–467. doi:10.1111/tpj.12485.

Arabidopsis thaliana tandem zinc finger 1 (AtTZF1) protein in RNA binding and decay

Jie Qu[1], **Shin Gene Kang**[1], **Wei Wang**[2,3], **Karin Musier-Forsyth**[2,3], and **Jyan-Chyun Jang**[1,4,5]

[1]Department of Horticulture and Crop Science, The Ohio State University, Columbus, OH 43210

[2]Department of Chemistry and Biochemistry, The Ohio State University, Columbus, OH 43210

[3]Center for RNA Biology, The Ohio State University, Columbus, OH 43210

[4]Department of Molecular Genetics, The Ohio State University, Columbus, OH 43210

[5]Center for Applied Plant Sciences, The Ohio State University, Columbus, OH 43210

SUMMARY

Arabidopsis thaliana Tandem Zinc Finger 1 (AtTZF1) protein is characterized by two tandem-arrayed CCCH type zinc fingers. We have previously found that AtTZF1 affects hormone-mediated growth, stress and gene expression responses. While much has been learned at the genetic and physiological level, the molecular mechanisms underlying the effects of AtTZF1 on gene expression remain obscure. A human TZF protein, hTTP, is known to bind and trigger the degradation of mRNAs containing AU-rich elements (AREs) at the 3′ untranslated regions. However, while the TZF motif of hTTP is characterized by $C_{X8}C_{X5}C_{X3}H$-$_{X18}$-$C_{X8}C_{X5}C_{X3}H$, AtTZF1 contains an atypical motif of $C_{X7}C_{X5}C_{X3}H$-$_{X16}$-$C_{X5}C_{X4}C_{X3}H$. Moreover, the TZF motif of AtTZF1 is preceded by a plant-unique arginine-rich (RR) region. Using fluorescence anisotropy and electrophoretic mobility shift binding assays, we have demonstrated that AtTZF1 binds to RNA molecules with specificity and the interaction is dependent on the presence of zinc. Compared to hTTP in which TZF is solely responsible for RNA binding, both TZF and arginine-rich (RR) regions of AtTZF1 are required to achieve high affinity RNA binding. Moreover, zinc finger integrity is vital for RNA binding. Using a plant protoplast transient expression analysis, we have further revealed that AtTZF1 can trigger the decay of ARE-containing mRNAs in vivo. Taken together, our results support the notion that AtTZF1 is involved in RNA turnover.

Keywords

Arabidopsis thaliana; arginine-rich (RR) motif; AtTZF1; AU-rich elements (AREs); Tandem CCCH Zinc Finger (TZF) motif; fluorescence anisotropy; RNA-binding; protein-RNA interaction; EMSA; RNA turnover

To whom correspondence should be addressed: Jyan-Chyun Jang. Address: 013 Rightmire Hall, 1060 Carmack Road, Columbus, OH 43210; Tel: (614)292-8496; Fax: (614) 247-8937; jang.40@osu.edu. Jie Qu, qu.20@buckeyemail.osu.edu. Shin Gene Kang, sgenek@gmail.com. Wei Wang, wangwei.chemistry@gmail.com. Karin Musier-Forsyth, musier-forsyth.1@osu.edu..

SUPPORTING INFORMATION

Additional supporting information may be found in the online version of this article.

INTRODUCTION

The zinc finger motif is a small protein motif that autonomously forms stable finger-like structures in the presence of one or more zinc cations (Klug and Schwabe 1995; Laity *et al.*, 2001). Zinc finger motif proteins are involved in diverse cellular function, such as transcription, mRNA degradation, protein-protein interaction and lipid binding (Laity *et al.*, 2001). According to the number and arrangement of cysteine and histidine residues, which are responsible for zinc coordination, zinc finger motifs can be classified as C_2H_2, C_2HC, C_2HC_5, C_3H, C_3HC_4, C_4, C_4HC_3, C_6, and C_8 (Berg and Shi 1996; Takatsuji 1998; Blackshear 2002; Moore and Ullman 2003; Jenkins *et al.*, 2005; Schumann *et al.*, 2007). Each type of zinc finger motif alone or in tandem gives rise to a unique structure that is associated with a specific function. For instance, Arabidopsis Transcription Factor IIIA (TFIIIA) binds to specific DNA regions via its C_2H_2 motifs, leading to enhanced transcription of 5S rRNA genes (Laity *et al.*, 2001; Mathieu *et al.*, 2003). The C_3HC_4 zinc RING finger of the Arabidopsis peroxin 10 (PEX10) provides an interface for protein-protein interaction, which is required for the attachment between peroxisomes and chloroplasts (Schumann *et al.*, 2007).

Tandem C_3H Zinc Finger (TZF) proteins belong to a small subfamily of the larger zinc finger family, with human Tristetraprolin (hTTP) as the prototype (Lai *et al.*, 1990; Worthington *et al.*, 1996; Lai *et al.*, 1999). The zinc finger motif of hTTP, also known as Nup475/TIS11/G0S24 (DuBois *et al.*, 1990; Lai *et al.*, 1990; Ma and Herschman 1991; Heximer and Forsdyke 1993), is characterized by two identical $C_{X8}C_{X5}C_{X3}H$ in tandem separated by 18 amino acids (Worthington *et al.*, 1996; Blackshear *et al.*, 2005). Nuclear Magnetic Resonance (NMR) structure analysis of TIS11d, a homolog of hTTP, has revealed that each C_3H zinc finger recognizes one 5′-UAUU-3′ subsite and two fingers symmetrically bind to two adjacent subsites (Hudson *et al.*, 2004). hTTP binds to the AU-rich elements (AREs) via its TZF motif at the 3′UTR of mRNAs encoding important regulators, such as Tumor Necrosis Factor-α (TNF-α) (Lai *et al.*, 1999; Lai and Blackshear 2001), granulocyte macrophage-colony stimulating factor (Carballo *et al.*, 2000; Lai and Blackshear 2001) and interleukin-3 (Lai and Blackshear 2001). hTTP binds to mRNAs, and triggers deadenylation and degradation (Brooks and Blackshear 2013; Fabian *et al.*, 2013), hence playing an important role in mRNA turnover. TZF proteins have also been identified in the budding yeast *Saccharomyces cerevisiae* (Puig *et al.*, 2005) and the nematode *Caenorhabditis elegans* (Pagano *et al.*, 2007; Farley *et al.*, 2008). Yeast TZFs (Cth1 and Cth2) also contain tandem $C_{X8}C_{X5}C_{X3}H$ motifs spaced by 18 amino acids (Puig *et al.*, 2008). Cth1 and Cth2 trigger mRNA degradation by binding to specific AREs in the 3′UTR of target mRNAs encoding proteins involved in iron-dependent pathways (Puig *et al.*, 2005; Pedro-Segura *et al.*, 2008; Puig *et al.*, 2008; Vergara *et al.*, 2011). Therefore, they play significant roles in iron homeostasis by modulating cellular metabolism in response to iron deficiency (Puig *et al.*, 2008). Unlike human and yeast TZFs, nematode TZF proteins are composed of two C_3H motifs with slightly different spacing patterns, $C_{X8\text{-}9}C_{X5}C_{X3}H$ and $C_{X8\text{-}10}C_{X5}C_{X3}H$ (Pagano *et al.*, 2007). They also bind to mRNA at U-rich regions and participate in coordinating axis polarization and germline differentiation in embryo development

(Schubert *et al.*, 2000; Cuenca *et al.*, 2003; DeRenzo *et al.*, 2003; Pagano *et al.*, 2007; Farley *et al.*, 2008).

A genome-wide sequence analysis has identified 67 and 68 C_3H zinc finger protein genes from rice and Arabidopsis, respectively (Wang *et al.*, 2008). Based on the number and the spacing between adjacent zinc finger motifs, rice *TZF* genes are classified into 9 subfamilies, while Arabidopsis *TZF* genes can be grouped into 11 subfamilies (Wang *et al.*, 2008). Among 26 Arabidopsis TZF proteins containing two zinc finger motifs, only AtC3H14 and AtC3H15 (Wang *et al.*, 2008; Pomeranz *et al.*, 2011a) contain the same TZF motif ($C_{X8}C_{X5}C_{X3}H$-$_{X18}$-$C_{X8}C_{X5}C_{X3}H$) as that in hTTP (Worthington *et al.*, 1996; Blackshear *et al.*, 2005). Nine members in rice subfamily I and eleven members in Arabidopsis subfamily IX encode proteins consisting of an atypical TZF motif, $C_{X7\text{-}8}$ $C_{X5}C_{X3}H$-$_{X16}$-$C_{X5}C_{X4}C_{X3}H$, which is specific to higher plants (Wang *et al.*, 2008; Pomeranz *et al.*, 2010; Pomeranz *et al.*, 2011a). In addition, a highly conserved plant-unique arginine-rich region containing a $C_{X5}H_{X4}C_{X3}H$ motif is located upstream of the TZF motif (Wang *et al.*, 2008; Pomeranz *et al.*, 2010; Pomeranz *et al.*, 2011a). Among rice TZF proteins, *Oryza sativa* Delay of the Onset of Senescence (OsDOS) affects hormone-mediated leaf senescence (Kong *et al.*, 2006), whereas OsTZF1 is involved in photomorphogenesis and responses to stress hormone ABA (Zhang *et al.*, 2012). OsTZF1 also affects growth and stress responses by modulating the expression of genes involved in homeostasis of reactive oxygen species (ROS). Notably, OsTZF1 binds to U-rich sequences in the 3′UTR of two potential target mRNAs *in vitro* (Jan *et al.*, 2013). Arabidopsis TZF proteins, including PIE1, AtSZF1/AtSZF2, SOMNUS, AtTZF1, AtTZF2 and AtTZF3, have been revealed to affect embryogenesis (Li and Thomas 1998), responses to salt stress (Sun *et al.*, 2007), light-dependent seed germination (Kim *et al.*, 2008), ABA/GA mediated growth and abiotic stress responses (Lin *et al.*, 2011), and ABA and JA responses (Lee *et al.*, 2012), respectively.

While much has been learned about the functions of plant TZF proteins at the genetic and physiological levels, whether or not they can bind to specific mRNAs and affect their stabilities remains unknown. Our previous work indicated that although recombinant AtTZF1 could bind to both DNA and RNA *in vitro*, it could not bind to a known ARE target of hTTP in electrophoretic mobility gel shift assays (Pomeranz *et al.*, 2010). Notably, these experiments were conducted by using recombinant AtTZF1 protein purified using denaturing and refolding process. To determine if AtTZF1-ARE interaction is compromised due to incorrect protein folding, additional experiments were conducted using recombinant AtTZF1 protein purified under native conditions. In this report, we present evidence of specific RNA binding activity of AtTZF1 using fluorescence anisotropy (Heyduk *et al.*, 1996) and electrophoretic mobility shift binding assays. We have also identified protein domains critical for high-affinity RNA binding. In contrast to hTTP, in which the TZF motif is solely responsible for binding, both the TZF motif and the arginine-rich (RR) region preceding TZF motif are required for high affinity RNA binding. Mutations of conserved cysteine residues within the RR-TZF motifs diminish the interactions, suggesting that zinc finger integrity is important for binding. Finally, we provide evidence to show that AtTZF1 can trigger the degradation of ARE-containing mRNA in vivo.

RESULTS

Recombinant full-length GST-AtTZF1 binds to specific RNA elements

Previously, His-tagged AtTZF1 proteins were produced in *Escherichia coli* and purified under denaturing conditions, due to their insolubility. After renaturation, AtTZF1 proteins were shown to bind to ribohomopolymer U in bead-binding assays (Pomeranz *et al.*, 2010). However, they failed to bind an ARE probe derived from TNF-α mRNA (Pomeranz *et al.*, 2010), a known target of hTTP (Lai *et al.*, 1999; Lai and Blackshear 2001). One possible explanation is that refolding of denatured His-AtTZF1 was not complete, hence compromising the binding affinity. To ameliorate this situation, protein expression constructs containing GST tags were used and shown to produce soluble recombinant AtTZF1 in bacteria (Figure 1a). The recombinant protein was detected by anti-AtTZF1 antibodies in a Western-blot analysis (Figure 1b). We first tested the ability of GST-AtTZF1 to interact with 6-carboxyfluorescein-labeled ribohomopolymerU (polyU) and ribohomopolymerA (polyA) (Table 1) using fluorescence anisotropy (FA) method, which was previously used to investigate RNA-TZF interactions (Blackshear *et al.*, 2003; Brewer *et al.*, 2004; Pagano *et al.*, 2007). The FA of fluorescein-labeled polyU was dramatically enhanced upon AtTZF1 binding (Figure 2a), indicating significant binding. The apparent dissociation constant (K_d) of AtTZF1 for polyU is 2270 nM (Table 2). However, when polyU was replaced by polyA, no discernible increase in FA was observed with 7 μM protein, suggesting no binding of AtTZF1 to polyA (K_d > 10 μM; Figure 2b). GST was used as a negative control, and did not form detectable complexes with either polyU or polyA (Figures 2a, b). To determine whether AtTZF1-RNA interaction requires zinc as its human counterpart hTTP, RNA binding affinity was also measured in reactions containing 0.5 mM ethylenediaminetetraacetic acid (EDTA), a chelating ligand that could effectively extract the zinc ions from AtTZF1. As indicated in Figure 2c, the absence of zinc caused no binding of AtTZF1 to polyU, suggesting that AtTZF1-RNA interaction is dependent on zinc presence.

Because a synthetic TZF fragment (amino acids 102-174) from hTTP was shown to interact with ARE ligands containing one or multiple minimal binding sites 5′-UUAUUUAUU-3′ (Worthington *et al.*, 2002; Blackshear *et al.*, 2003), we tested if GST-AtTZF1 could bind ARE elements. Since a 1:1 stoichiometry of hTTP TZF:RNA can only be achieved with RNA elements as small as 9-13 nucleotides (Brewer *et al.*, 2004), ARE_{13} (5′-AUUUAUUUAUUUA-3′) was used as a positive control (Table 1). A mutated ARE probe, MutG (5′-UGUUUGUUGUUUGUUUGUU-3′), was used as a negative control based on previous finding that replacing one of the A residues with G, leaving three intact Us, significantly reduced RNA binding ability of hTTP TZF domain (Brewer *et al.*, 2004). Consistent with previous results (Brewer *et al.*, 2004), recombinant hTTP TZF fragment was able to bind to ARE_{13} (Figure S1a) and ARE_{19} (Figure S1b). A K_d of 200 nM for ARE_{13} and 340 nM for ARE_{19} were measured, respectively (Table 3). When MutG was used as a probe, there was no interaction between hTTP TZF fragment and MuG in FA analysis (Table 3). RNA electrophoretic mobility shift assays (EMSAs) were also used to examine hTTP TZF binding activity. Results confirmed that hTTP TZF bound to ARE_{19} with much higher affinity than MutG (Figure S2). Interestingly, full-length GST-AtTZF1 failed to interact with ARE_{13} (Table 2), but bound to a longer probe ARE_{19} with a K_d of 4550 nM

(Figure 3a and Table 2). Binding specificity to ARE_{19} was supported by lack of interaction with free GST and weak interaction with MutG (Figures 3a, b). RNA EMSAs also detected a modest interaction between AtTZF1 and ^{32}P-labeled ARE_{19} (Figure 4a). By contrast, AtTZF1 did not interact with ^{32}P-labeled MutG (Figure 4b). The specificity of the AtTZF1-ARE_{19} interaction was evaluated by competition with unlabeled ARE_{19}. As shown in Figure 4c, AtTZF1-ARE_{19} complexes were significantly diminished upon addition of unlabeled ARE_{19} in excess. Moreover, AtTZF1-ARE_{19} complex formation was shown to depend on the presence of zinc (Table 4). Taken together, full-length AtTZF1 binds to specific RNA elements in a zinc-dependent manner and acts as a weaker RNA-binding protein compared to the TZF domain of hTTP.

RNA binding characteristics of TZF motifs from hTTP, AtC3H15 and AtTZF1

Sequence comparison between tandem CCCH zinc finger proteins from human, yeast, nematode and Arabidopsis revealed that they share similarities in TZF region (Figure S3). Arabidopsis TZF proteins AtC3H14 and AtC3H15 share the same CCCH spacing pattern with hTTP (Figure S3). By contrast, members in the AtTZF gene family, including AtTZF1, encode proteins with a plant-unique TZF variant of $C_{X7\text{-}8}C_{X5}C_{X3}H\text{-}_{X16}\text{-}C_{X5}C_{X4}C_{X3}H$ (Pomeranz *et al.*, 2011a). To determine if the plant TZF motif is responsible for RNA binding, we tested AtTZF1 TZF fragment alongside with hTTP TZF fragment as a positive control (Figure 5a). Given that AtTZF1 contains an atypical TZF motif, AtC3H15 TZF fragment was included for comparison (Figure 5a). Because soluble GST fusion proteins of deleted AtTZF1 could not be produced, an MBP tag was used to create all TZF fragment fusion proteins. Both polyU and ARE_{19} were tested for binding as full-length AtTZF1 specifically bound to these RNAs (Table 2). The K_d for hTTP TZF and AtC3H15 TZF fragments binding to ARE_{19} was 340 nM and 130 nM (Figure 5b and Table 3), respectively, suggesting that the $C_{X8}C_{X5}C_{X3}H\text{-}_{X16}\text{-}C_{X8}C_{X5}C_{X3}H$ motif from plant was able to bind to RNA as its human counterpart. Moreover, AtC3H15 TZF fragment binding to ARE was dependent on zinc (Table 4). The hTTP TZF was found to bind polyU with a much lower affinity (K_d = 2290 nM) (Table 3), consistent with the notion that hTTP TZF fragment displays a strong preference for ARE over polyU (Brewer *et al.*, 2004). AtC3H15 TZF fragment did not bind to polyU (K_d >10 μM; Table 3), whereas AtTZF1 TZF fragment failed to bind to ARE_{19} (K_d > 10 μM) and could only bind to polyU poorly (K_d = 7370 nM) (Table 3). Similar binding results were observed when EMSAs were used to test hTTP TZF, AtC3H15 TZF and AtTZF1 TZF binding to ^{32}P-labeled ARE_{19} (Figure S4). Therefore, we conclude that while the plant TZF motif of $C_{X8}C_{X5}C_{X3}H\text{-}_{X18}\text{-}C_{X8}C_{X5}C_{X3}H$ is sufficient for RNA binding, the $C_{X7\text{-}8}C_{X5}C_{X3}H\text{-}_{X16}\text{-}C_{X5}C_{X4}C_{X3}H$ motif is not.

Both arginine-rich (RR) and TZF domain of AtTZF1 are required for high affinity RNA binding

As mentioned earlier, plant TZFs contain an extremely conserved arginine-rich (RR) region of 50 amino acids preceding the TZF motif (Pomeranz *et al.*, 2010). The RR region is highly enriched with basic amino acid residues (highlighted in purple in Fig. S5), which is typically involved in RNA binding (Bayer *et al.*, 2005; Lunde *et al.*, 2007). *In silico* analysis of the primary RR-TZF domain structure via BindN (Wang and Brown 2006) and RNABindR (Walia *et al.*, 2012) revealed multiple putative RNA-binding residues in the RR-TZF

domain (Figure 6a), suggesting that the RR-TZF domain might be important for RNA-binding. To test this hypothesis, recombinant MBP-tagged AtTZF1 RR, TZF and RR-TZF fragments (Figure 6b) were used to determine the binding affinity of each domain with polyU and ARE_{19} using FA analysis. Results showed that neither RR nor TZF domain alone conferred detectable binding to RNA molecules tested (Figure 6c and Table 3). However, the RR-TZF domain could bind both polyU and ARE_{19} with a K_d of 470 nM and 410 nM (Table 3), respectively. This was further supported by the results that RNA-binding activity was partially reconstituted when separate RR domain and TZF domain were mixed *in vitro* (Table 3), particularly evident for the interaction with ARE_{19} (Figure 6c). EMSA experiments were carried out to verify RNA binding trends. An increase in RR-TZF concentration caused a shift of ^{32}P-labeled ARE_{19}, as indicated in Figure 7a. Protein-RNA aggregates were also observed in the loading wells. By contrast, no specific protein-RNA complexes that entered the gel were detected when ARE_{19} was replaced by MutG although this probe also triggered protein-RNA aggregation in the wells (Figure 7b). In addition, neither RR nor TZF domains alone bound to ARE_{19} in a specific manner (Figures 7c, d). Collectively, these results suggest that both RR and TZF domains are required for specific AtTZF1-RNA interaction.

The effect of zinc on RR-TZF binding to RNA was also evaluated. In the absence of zinc, the binding affinity was increased from 470 nM to 3200 nM (Table 4), implying severely reduced interaction between RR-TZF and polyU. For ARE_{19}, RR-TZF also displayed higher affinity in the presence of zinc (K_d = 410 nM) than in the absence of zinc (K_d = 2910 nM) (Table 4). In conclusion, the interaction between RR-TZF fragment and RNA is much stronger in the presence of zinc.

Zinc finger integrity is important for AtTZF1-RNA interaction

The zinc-dependent interaction observed between full-length AtTZF1 and RNA (Table 4) suggests that AtTZF1·RNA complex formation may be mediated through zinc fingers. To test this hypothesis, a series of site-directed full-length AtTZF1 mutants that contain single or multiple cysteine to arginine changes within RR-TZF region were tested (Figure 8a). As mutation of single cysteine to arginine in key CCCH residues of either zinc finger completely abrogated hTTP TZF domain binding to AREs (Lai *et al.*, 2002), we first generated an full-length AtTZF1 double mutant C136R/C171R, in which the first cysteine in each CCCH zinc finger was mutated to arginine. In addition to the TZF motif, the RR region of AtTZF1 contains a plant-specific $C_{X5}H_{X4}C_{X3}H$ motif, which is predicted to be a zinc finger. Therefore, a full-length mutant (C101R) containing a single cysteine to arginine mutation in the $C_{X5}H_{X4}C_{X3}H$ motif, and a full-length triple mutant containing both C101R and C136R/C171R were also generated. Both polyU and ARE_{19} were assayed for protein-RNA interaction. Compared to WT full-length AtTZF1, none of the mutant proteins could interact with ARE_{19} (Figure 8b) and polyU (Table 2), suggesting that the integrity of the CHCH motif and the TZF motif are both important for full-length AtTZF1-RNA association.

Site-directed mutagenesis was also applied to the RR-TZF domain. Both FA and EMSA analyses were used to measure binding affinity of RR-TZF mutants to RNA elements. In FA

experiments, the binding affinities of C101R/C136R/C171R mutant for either polyU (K_d = 3100 nM) or ARE_{19} (K_d = 3030 nM) were greatly compromised compared to that of WT RR-TZF (470 nM for polyU and 410 nM for ARE_{19}) (Table 3). By contrast, single (C101R) or double (C136R/C171R) mutation affected RR-TZF binding activities to a lesser extent. For instance, the K_d for polyU was only slightly increased from 470 nM (WT) to 810 nM for single mutant and to 1610 nM for double mutant (Table 3). Nevertheless, a double mutant was more effective in weakening RNA-binding activity of RR-TZF than a single mutant. In EMSAs (Figure 9), none of the RR-TZF mutants could form specific protein-ARE_{19} complexes, although RNA-protein aggregates were present in the loading wells. Taken together, both RR and TZF domains appear to be required for specific AtTZF1-RNA complex formation.

The effects of AtTZF1 on mRNA stability and accumulation

To determine the impact of AtTZF1-RNA interaction in vivo, a maize protoplast transient expression system (Sheen 2001) was used to determine mRNA stability and accumulation. In this analysis, AtTZF1-mCherry was used as an effector and GFP-GASA6-ARE was used as a reporter. hTTP-mCherry and GFP-GASA6-MutG were used as a positive effector control and a negative reporter control, respectively (Figure 10a). *GASA6* (At1g74670) encodes a small peptide of 101 aa (Lin *et al.*, 2011). The four independent constructs and free GFP were expressed at similar high levels, indicating no endogenous constraints for their expression (Figures 10b and S6). Protoplast samples were co-transformed with a distinct pair of effector and reporter, and incubated for 10 h before time course mRNA half-life experiments were conducted using actinomycin D (100 μg/ml) to block the transcription. Results showed that AtTZF1 and hTTP could both increase the K_{decay} and decrease the $T_{1/2}$ of GFP-GASA6-ARE mRNA, respectively (Figures 10c, d). The changes were not due to general decline of mRNA half-lives because neither mCherry fusion constructs nor endogenous control PP2A were affected (Figure S7). Furthermore, neither effectors had any significant effects on mutant reporter GFP-GASA6-MutG mRNA stability (Figures 10c, d), indicating that accelerated GFP-GASA6-ARE mRNA decay was due to specific protein-RNA interaction.

Protoplast samples were also collected after 14 h incubation without actinomycin D treatments to determine the effects of AtTZF1 and hTTP on mRNA and protein accumulation. Consistent with mRNA half-life assays (Figure 10) and fluorescence microscopy results (Figure 11a), GFP-GASA6-ARE mRNA accumulation was significantly reduced in the presence of AtTZF1-mCherry and hTTP-mCherry (Figure 11b). The GFP-GASA6-MutG mRNA accumulation was comparable among different samples, except it was higher in the presence of AtTZF1-mCherry. Results of Western blot analysis confirmed that AtTZF1 and hTTP could reduce GFP-GASA6-ARE accumulation (Figure 11c). Collectively, these results indicate that, similar to hTTP (Brooks and Blackshear 2013), AtTZF1 not only bind but also trigger turnover of ARE-containing mRNAs.

DISCUSSION

Post-transcriptional regulation plays an essential role in gene expression by modulating mRNA transport (Vargas *et al.*, 2005), localization (Martin and Ephrussi 2009), stability (Garneau *et al.*, 2007) and translation (Muench et al., 2012; Wells 2012). These regulated processes are mediated through the interactions between specific mRNA elements and RNA-binding proteins (Lunde *et al.*, 2007; Licatalosi and Darnell 2010; Tam *et al.*, 2010). A well-documented example is AREs in the 3′UTR of many mRNAs acting as determinants of RNA stability in mammalian cells (Barreau *et al.*, 2005). Among ARE-interacting proteins, mammalian TZFs (TTP, TIS11b, and TIS11d) can promote the degradation of mRNAs encoding regulators involved in innate immune responses (Lai *et al.*, 2000; Raghavan *et al.*, 2001; Worthington *et al.*, 2002). Budding yeast TZFs (Cth1 and Cth2) are also ARE-binding proteins, and they control the half-lives of mRNAs that encode proteins involved in iron-dependent pathways (Puig *et al.*, 2005; Pedro-Segura *et al.*, 2008; Puig *et al.*, 2008; Vergara *et al.*, 2011). Nematode TZFs (MEX-5, MEX-6 and POS-1) confer RNA binding affinity; however, they interact preferentially with U-rich consensus elements, which are remarkably abundant in the 3′UTR of *C.elegans* transcripts (Pagano *et al.*, 2007; Farley *et al.*, 2008). As for plant TZFs, only AtTZF1 and OsTZF1 have been reported to be RNA-binding proteins (Pomeranz *et al.*, 2010; Jan *et al.*, 2013). OsTZF1 binds to U-rich and ARE-like motifs in the 3′UTR of two transcripts that are down-regulated in OsTZF1 over-expression plants (Jan *et al.*, 2013). Here we have demonstrated that AtTZF1 binds to polyU and ARE_{19} with specificity. Additionally, we have identified a unique RNA-binding domain containing both RR and TZF domains responsible for higher strength AtTZF1-RNA interaction. Moreover, zinc finger integrity is important to achieve high-affinity RNA binding activity of AtTZF1. Finally, we show that AtTZF1 can trigger degradation of ARE-containing mRNAs.

NMR structure analysis of TIS11d-RNA complexes has provided insights into the molecular mechanisms by which the TZF domain binds ARE elements (e.g., 5′-UUAUUUAUU-3′) (Hudson *et al.*, 2004). This interaction is largely achieved through a network of hydrogen bonds between functional groups of protein backbone and the Watson-Crick edges of the bases. It is also stabilized by intercalative stacking between conserved aromatic side chains of TIS11d and the RNA bases (Hudson *et al.*, 2004). Apart from key CCCH residues, the highly conserved lead-in motif immediately preceding the first cysteine of each CCCH zinc finger (Figures S3 and S5) forms two sidewalls of a deep pocket accommodating both U and A bases at the 5′ end of each UAUU site (Hudson *et al.*, 2004). Finally, conservation is found in several critical amino acid residues with aromatic side chains (i.e., Tyr170, Phe176, Tyr208, and Phe214) (Figure S3). Each of which is sandwiched between two adjacent aromatic RNA bases (Hudson *et al.*, 2004; Pomeranz *et al.*, 2011a). A more recent report has shown that deletion or addition of a single residue within the C-$_{X8}$-C interval of finger 1 and the C-$_{X5}$-C or C-$_{X3}$-C interval of either finger greatly reduced RNA binding affinity of hTTP (Lai *et al.*, 2013). Furthermore, charge reversal mutations within the conserved RYKTEL region preceding the first C had a strong negative impact on hTTP-RNA assembly (Lai *et al.*, 2013). Therefore, the lack of a detectable interaction between the isolated TZF domain of AtTZF1 and a consensus ARE_{19} is likely due to the lack of conservation in CCCH spacing pattern, lead-in sequences, and critical aromatic residues (Pomeranz *et al.*,

2011). This notion is further supported by our findings in which the TZF domain of AtC3H15, but not AtTZF1, binds to ARE_{19}; because only AtC3H15 contains exactly the same spacing and conserved lead-in sequence as hTTP. Moreover, all four conserved aromatic residues are present in the AtC3H15 TZF but only two are present in the AtTZF1 TZF (Figure S3).

Although the AtTZF1 TZF domain alone is insufficient for high-affinity RNA-binding, we have found that the TZF domain appended to an additional RR domain displays RNA-binding activity. Interestingly, the RR domain alone doesn't bind RNA molecules either; however, when RR is added to TZF in trans, binding is observed. This result suggests that covalent continuity is not a requirement for RR-TZF binding. Moreover, mutations disrupting either the RR domain or the TZF domain cause significant decrease in binding affinity, supporting the idea that both RR and TZF are required for RNA binding. This is not unprecedented because similar mechanisms have been observed in other RNA-binding zinc finger proteins, such as HIV-1 Nucleocapsid (NC) protein NCp7 (Dannull *et al.*, 1994) and the 30-kD subunit of Arabidopsis Cleavage and Polyadenylation Specificity Factor AtCPSF30 (Delaney *et al.*, 2006). For example, NCp7 contains two CCHC zinc fingers, of which the first is flanked by two clusters of basic amino acids (Dannull *et al.*, 1994). Mutations of either the conserved basic residues or the zinc finger motifs greatly affect NCp7 binding to specific RNA elements (Dannull *et al.*, 1994; Schmalzbauer *et al.*, 1996), indicating that the zinc fingers and flanking basic residues both contribute to RNA binding. On the other hand, although domains outside the TZF motif can enhance RNA binding, they may also have negative effects. This is evidenced by lower RNA binding affinity of full-length AtTZF1 relative to that of the RR-TZF domain.

In hTTP, the TZF domain is solely responsible for RNA binding (Blackshear *et al.*, 2003). Absence of zinc or mutations in the zinc fingers abolishes the interaction between the hTTP TZF domain and AREs (Lai *et al.*, 2002; Brewer *et al.*, 2004). By contrast, the TZF domain is necessary, but not sufficient for AtTZF1 to bind RNA. Nevertheless, RNA binding activities are significantly diminished by either zinc depletion or mutations that disrupt zinc finger structures for the full-length AtTZF1, suggesting that zinc finger integrity is important for RNA binding. Interestingly, in FA analyses, the RR-TZF domain appears to bind to RNA independent of zinc; except for the triple mutation (C101R/C136R/C171R), neither C101R nor C136R/C171R changes affect RNA binding significantly. However, we were unable to detect a specific interaction between any RR-TZF mutant and ARE_{19} by EMSA. The discrepancy between FA and EMSA results may be due to the fact that RR-TZF proteins aggregate with RNA in a non-specific manner at high concentration, because they are positively charged in the neutral binding environment (protein isoelectric point of RR-TZF is 9.53). These aggregates were clearly observed by EMSA for all variants. FA values are skewed due to the formation of protein-RNA aggregates when protein concentration is increased, which is indicated by a drastic decrease in fluorescence intensity. Therefore, in this case, EMSA results are more reliable in characterizing RR-TZF-RNA interaction, revealing that any mutation to disrupt the zinc fingers abolishes specific RNA-binding activity. This is also consistent with FA results from mutational analyses of full-length AtTZF1.

Although spacing patterns of TZF domains are not conserved between plants and mammals, it has long been speculated that plant TZF proteins can not only bind RNA, but also be involved in RNA regulation (Lin *et al.*, 2011; Pomeranz *et al.*, 2011a; Pomeranz *et al.*, 2011b; Jan *et al.*, 2013). Using a plant protoplasts transient expression system, we have demonstrated that AtTZF1 can trigger the degradation of ARE-containing mRNAs. It appears that the degree of RNA decay is directly correlated with RNA binding capacity, i.e., compared to hTTP, AtTZF1 binds less strongly to ARE and hence less effective in RNA turnover. Nevertheless, these results are convincing enough to suggest that AtTZF1 can indeed trigger RNA degradation in plant cells. Because AtTZF1's true targets are unknown, it is currently impossible to evaluate if AtTZF1 can be as effective as hTTP in RNA regulation. Future work should focus on the global identification of AtTZF1's target mRNAs and in vivo binding sites.

EXPERIMENTAL PROCEDURES

Molecular cloning

An in-frame fusion of GST-AtTZF1 was generated by subcloning full-length AtTZF1 cDNA into pGEX-KG vector (Guan and Dixon 1991) via *BamH*I and *EcoR*I sites. Single (C101R), double (C136R/C171R) and triple (C101R/C136R/C171R) cysteine to arginine mutation of AtTZF1 were created using QuickChange™ site-directed mutagenesis kit (Stratagene, Santa Clara, CA) following manufacturer's instructions. Mutated *AtTZF1* cDNAs were similarly cloned into pGEX-KG vector. For the deletion analysis, fragments of *AtTZF1* containing the arginine-rich (RR) domain (amino acids 86-128), the TZF domain (amino acids 129-195) and the RR-TZF domain (amino acids 86-195), respectively, were subcloned into pMAL-C2X vector (New England Biolabs, Ipswich, MA) between *EcoR*I and *Hind*III, which generated MBP-RR, MBP-TZF, and MBP-RR-TZF construct, respectively. *AtTZF1* deletion fragments with point mutations, including RR (C101R), TZF (C136R/C171R), RR-TZF (C101R/C136R/C171R) were amplified from corresponding full-length *AtTZF1* mutants and sub-cloned into pMAL-C2X vector via *EcoR*I and *Hind*III sites. An *hTTP* fragment containing TZF domain (amino acid 109-181) (Pomeranz *et al.*, 2010) was sub-cloned into pMAL-C2X vector between *EcoR*I and *Hind*III sites. A TZF motif fragment (amino acid 221-294) of *AtC3H15* (*At1g68200*) was also sub-cloned into pMAL-C2X vector via *Pst*I and *EcoR*I sites. All the constructs were sequenced and verified prior to transforming to *E. coli* for recombinant protein production.

For DNA constructs used in mRNA half-life assays, *GASA6-ARE* was made by ligating the ARE (5′-TTATTTATTATTTATTTATTATTTATTTATTATTTATTTATTA^{28}-3′) to the end of *GASA6* (At1g74670) coding region via PCR, subcloning to TOPO-D vectors (Life technologies, Grand Island, NY), and then transferring to Gateway-compatible pBluescript KS+ vectors by recombination reactions (Pomeranz *et al.*, 2010). GFP-GASA6-MutG was generated following the same procedures except the ARE region was replaced by the MutG (5′-TTGTTTGTTGTTTGTTTGTTGTTTGTTTGTTGTTTGTTTGTTA^{28}-3′). hTTP-mCherry was generated by transferring hTTP coding sequence in pENTR3C vectors to mCherry vector via recombination reactions (Pomeranz *et al.*, 2010). Oligo primers used for molecular cloning are listed in Table S1.

Recombinant protein production

Fusion proteins were produced using BL21DE3 (codon plus) cells. Bacterial cultures were grown to A_{600}=0.6, at which point IPTG was added to final concentration of 0.1 mM for induction of protein production. Glucose was added to LB medium to a final concentration of 0.2% (w/v) for MBP-tagged fusion protein induction. After induction, bacterial cultures were grown at 18°C for 12-16 h before harvest. Protein expression was determined by Coomassie-stained SDS-PAGE gels as described (Blackshear 1984; Westermeier 2006). GST fusion proteins were purified using glutathione-Sepharose 4B resin (GE Healthcare Biosciences, Pittsburgh, PA). Bacterial cells from 2 L culture were collected by centrifugation at 4,000 rpm for 20 min and resuspended in lysis buffer [50 mM Tris-HCl, pH 7.3, 400 mM NaCl, 1 mM PMGF, 1X plant protease inhibitor (0.2 mM AEBSF, 0.7 μM Bestatin, 0.7 μM Pepstatin A, 10 μM Leupeptin, 1.4 μM E-64, 1.4 μM Phenanthroline)]. Lysozyme was added to a final concentration of 1 mg/ml and the cell suspension was incubated on ice for 30 min. Triton X-100 to a final concentration of 0.2% was then added and the culture was subjected to vigorous rocking for another 10 min at 4 °C. Sonication was then applied to further lyse the cells using Sonicator (180W, 3 s pulse, 20 times; Sonics & Materials Inc., Newtown, CT), followed by centrifugation at 10,000 rpm for 30 min. The supernatant (cell lysate) was collected and incubated with 2 ml 50% slurry of glutathione-agarose resin in lysis buffer for 2 h. A total of 100 ml lysis buffer was used to wash the resin three times before elution. Three 3 ml fractions of GST fusion proteins were eluted sequentially from the resin using glutathione elution buffer (50 mM Tris-HCl, pH 8.0, 100 mM NaCl, 10 mM reduced glutathione). Fractions containing GST fusion proteins were pooled and dialyzed using dialysis buffer (20 mM Tris-HCl, pH 8.0, 50 mM NaCl, 1mM DTT). After dialysis, the protein concentration was determined by the Bradford method (Kruger 2002). Proteins were concentrated by Amiscon™ protein concentrator (EMD Millipore Corporation, Billerica, MA) to ~20 μM before storage in 100 μl aliquots at −80°C. Western blot analysis of recombinant GST-AtTZF1 was conducted by using AtTZF1 antibodies as previously described (Jang *et al.*, 2000). MBP fusion proteins were purified using amylase-agarose beads (New England Biolabs, Ipswich, MA) following the same protocol as used for GST fusion proteins. Instead of using glutathione elution buffer, the fusion proteins were eluted by maltose elution buffer (50 mM Tris-HCl, pH 8.0, 50 mM NaCl, 10 mM maltose).

RNA substrates

For FA assays, RNA oligonucleotides were chemically synthesized and labeled with 6-carboxyfluorescein (FAM) at the 5′ end (Integrated DNA Technology, Coralville, IA). Lyophilized RNA was dissolved in diethyl pyrocarbonate (DEPC)-treated water and quantified by absorbance at 260 nM via a NanoDrop™ ND-2000 (Thermo Scientific, Wilmington, DE). Ten microliter aliquots containing 10 μM RNA molecules was prepared and stored at −80°C. For EMSA, RNA oligonucleotides (Integrated DNA Technologies, Coralville, IA) were radiolabeled using T4 polynucleotide kinase (New England Biolabs, Ipswich, MA) and [γ-^{32}P]ATP (100 μCi/μmol) (PerkinElmer Life Sciences, Waltham, MA) to specific activities of 1-2 × 10^5 cpm/fmol. ^{32}P-labeled probes were separated on 15% denaturing urea gels. Full-length RNAs were excised and eluted in DEPC-treated water

overnight. Following butanol extraction, RNAs were precipitated with 100% ethanol in the presence of 3 M NaOAC at −80 °C for 2 h, collected by centrifugation, dissolved in DEPC-water, and monitored by scintillation counting. The sequences of RNA substrates are listed in Table 1.

Fluorescence anisotropy assays

Fluorescence anisotropy (FA) assays were carried out to determine the binding affinity of recombinant proteins to 6-FAM-labeled RNA oligonucleotides. RNA (20 nM) and a specific concentration of protein was equilibrated in binding buffer (20 mM HEPES, pH 7.5, 50 mM NaCl, 5 mM 2-mercaptoethanol, 1 mM DTT) at 25°C for 30 min. Where applicable, $ZnCl_2$ (5 μM) or EDTA (0.5 mM) was included in the reactions. Prior to the addition of RNA substrates, proteins were incubated in the binding mixture for 15 min at 25°C to allow coordination or chelation of Zn^{2+}. FA measurements were conducted using an Analyst AD plate reader system (Molecular Devices, Sunnyvale, CA) using Corning 3676 low-volume 384-well black nonbinding-surface polystyrene plates (Corning Inc., Tewksbury, MA). Samples were excited at 490 nm and the emission (520 nm) intensities from the parallel and perpendicular planes were measured. Four readings were measured for each experiment. The mean and standard deviation of the anisotropy value (r) were calculated for each protein concentration. To determine the equilibrium dissociation constants (K_d), the FA data were fit to Equation 1 (Stewart-Maynard *et al.*, 2008) as a function of protein concentration according to the expression,

$$A(C) = \frac{A_B + \theta(A_B R - A_B)}{\theta(R-1)+1} \quad \text{(Eq.1)}$$

where

$$\Theta = \frac{1}{2D}\left[D + C + K_d - \sqrt{(D+C+K_d)^2 - 4C \cdot D}\right.$$

is the fraction of bound oligonucleotides, and D is the concentration of oligonucleotides. A_B and A_F are the FA values of maximally bound and unbound oligonucleotides, respectively. R represents the ratio of the fluorescence intensity of fully bound oligonucleotides relative to free oligonucleotides, which reflects changes in fluorescence intensity upon protein binding. The reported value in each table was an average of three independent experiments and the reported error was the standard deviation.

RNA electrophoretic mobility shift assays

Binding reactions were performed by incubating ^{32}P-labeled RNAs (4,000 cpm) with increasing concentrations (indicated in Figures) of recombinant protein at RT for 30 min in 10 μl of binding buffer containing 20 mM HEPES, pH 7.5, 50 mM NaCl, 5 mM 2-mercaptoethanol, 1 mM DTT, 5 μM $ZnCl_2$, and 4 mM $MgCl_2$. Electrophoresis was performed at 4 °C in 8% native Tris borate-acrylamide (29:1) gels, which were fixed, dried, and exposed overnight in a Phosphor Imager cassette. Results were visualized by a Typhoon Trio Molecular Imager (GE Healthcare Bio-Sciences, Piscataway, NJ). For competition

assays, ^{32}P-labeled RNAs and recombinant protein were incubated prior to the addition of unlabeled competitor RNA.

mRNA half-life assays

A maize protoplast transient expression system was used for this analysis (Sheen 2001). Protoplast preparation and transformation were conducted as described (Pomeranz *et al.*, 2010). Protoplast samples were co-transformed with a distinct pair of effector and reporter (TZF1+ARE, TZF1+MutG, hTTP+ARE, hTTP+MutG). For the reporter-only samples, protoplasts were co-transformed with each reporter (ARE or MutG) and a non-specific plasmid DNA (equivalent amount to the effector). After 10 h incubation in the dark at 25°C, Actinomycin D (Sigma-Aldrich, St.Louis, MO) was added to a final concentration of 100 μg/ml to block transcription. Protoplasts were collected prior to Actinomycin D treatment (0 h), and then at 1, 2 and 4 h after treatment.

Total RNA was isolated using the RNeasy plant mini kit (QIAGEN, Gaithersburg, MD), followed by genomic DNA removal using DNA-free™ kit (Ambion, GrandIsland, NY). cDNA was prepared from 0.25 μg of total RNA using oligo $(dT)_{20}$ primers and SuperScript III reverse transcriptase (Invitrogen, Grand Island, NY) according to the manufacturer's protocol. RT reactions were diluted 4-fold and 3 μl of the dilutions were used for subsequent PCR reactions. Real time PCR was performed using iQ SYBR Green Supermix and an iQ-Cycler instrument (BioRad Laboratories Inc., Hercules, CA) in 15 μl reactions. The following PCR condition was used: 94°C for 2min, followed by 40 cycles of 94°C for 15 s and 60 °C for 34 s (Kim and Somers 2010). Primers used in quantitative RT-PCR were listed in Table S2.

Each cDNA sample in mRNA half-life assays was analyzed in duplicate, and transcript abundance was described as a ratio relative to expression levels before actinomycin D treatment (0 h), which was set to a value of 1.0. The mRNA decay has been found to obey first-order kinetics in general (Ross 1995; Gutierrez *et al.*, 2002; Narsai *et al.*, 2007). Therefore, an exponential regression model ($A = \theta^{-kt}$) was used to fit the data and calculate K_{decay} for each transcript. The mRNA half-life ($T_{1/2}$) was then calculated using the equation $T_{1/2}=\frac{ln\,(2)}{K_{decay}}$. Mean value and standard deviation of K_{decay} were calculated from two biological replicates. Student t-test was conducted to evaluate the differences in K_{decay} between different samples.

The cDNA samples used for RNA accumulation analysis (without actinomycin D treatment) were analyzed in triplicate, and the expression levels of GASA6 or mCherry were normalized to that of *PP2A* (Protein Phosphatase 2A Subunit A3) (Livak and Schmittgen 2001; Czechowski *et al.*, 2005). Protein isolation and gel-blot analyses were carried out as described (Jang *et al.*, 2000).

Supplementary Material

Refer to Web version on PubMed Central for supplementary material.

ACKNOWLEDGEMENTS

We thank the Arabidopsis Biological Resource Center (Columbus, OH) for providing cDNA clones, Dr. Desh Verma for providing pGEX-KG vector, Dr. Meng Sun for technical help in FA experiments, Drs. Esther van der Knaap and Eric Stockinger for critical reading of the manuscript. This work is supported by the National Science Foundation IOB-0543751 (to J.-C.J.), Ohio Plant Biotech Consortium OHOA 0794 (to J.-C.J.) and National Institutes of Health RO1 GM065056 (to K.M.-F.).

REFERENCES

Barreau C, Paillard L, Osborne HB. AU-rich elements and associated factors: are there unifying principles? Nucleic Acids Res. 2005; 33:7138–7150. [PubMed: 16391004]

Bayer TS, Booth LN, Knudsen SM, Ellington AD. Arginine-rich motifs present multiple interfaces for specific binding by RNA. RNA. 2005; 11:1848–1857. [PubMed: 16314457]

Berg JM, Shi Y. The galvanization of biology: a growing appreciation for the roles of zinc. Science. 1996; 271:1081–1085. [PubMed: 8599083]

Blackshear PJ. Systems for polyacrylamide gel electrophoresis. Methods Enzymol. 1984; 104:237–255. [PubMed: 6717283]

Blackshear PJ. Tristetraprolin and other CCCH tandem zinc-finger proteins in the regulation of mRNA turnover. Biochem Soc Trans. 2002; 30:945–952. [PubMed: 12440952]

Blackshear PJ, Lai WS, Kennington EA, Brewer G, Wilson GM, Guan X, Zhou P. Characteristics of the interaction of a synthetic human tristetraprolin tandem zinc finger peptide with AU-rich element-containing RNA substrates. J Biol Chem. 2003; 278:19947–19955. [PubMed: 12639954]

Blackshear, PJ.; Phillips, RS.; Lai, WS. Tandem CCCH Zinc Finger Proteins in mRNA Binding Georgetown. Kluwer Academic/Plenum Publishers; New York: 2005.

Brewer BY, Malicka J, Blackshear PJ, Wilson GM. RNA sequence elements required for high affinity binding by the zinc finger domain of tristetraprolin: conformational changes coupled to the bipartite nature of Au-rich MRNA-destabilizing motifs. J Biol Chem. 2004; 279:27870–27877. [PubMed: 15117938]

Brooks SA, Blackshear PJ. Tristetraprolin (TTP): interactions with mRNA and proteins, and current thoughts on mechanisms of action. Biochim Biophys Acta. 2013; 1829:666–679. [PubMed: 23428348]

Carballo E, Lai WS, Blackshear PJ. Evidence that tristetraprolin is a physiological regulator of granulocyte-macrophage colony-stimulating factor messenger RNA deadenylation and stability. Blood. 2000; 95:1891–1899. [PubMed: 10706852]

Cuenca AA, Schetter A, Aceto D, Kemphues K, Seydoux G. Polarization of the C. elegans zygote proceeds via distinct establishment and maintenance phases. Development. 2003; 130:1255–1265. [PubMed: 12588843]

Czechowski T, Stitt M, Altmann T, Udvardi MK, Scheible WR. Genome-wide identification and testing of superior reference genes for transcript normalization in Arabidopsis. Plant Physiol. 2005; 139:5–17. [PubMed: 16166256]

Dannull J, Surovoy A, Jung G, Moelling K. Specific binding of HIV-1 nucleocapsid protein to PSI RNA in vitro requires N-terminal zinc finger and flanking basic amino acid residues. EMBO J. 1994; 13:1525–1533. [PubMed: 8156990]

Delaney KJ, Xu R, Zhang J, Li QQ, Yun KY, Falcone DL, Hunt AG. Calmodulin interacts with and regulates the RNA-binding activity of an Arabidopsis polyadenylation factor subunit. Plant Physiol. 2006; 140:1507–1521. [PubMed: 16500995]

DeRenzo C, Reese KJ, Seydoux G. Exclusion of germ plasm proteins from somatic lineages by cullin-dependent degradation. Nature. 2003; 424:685–689. [PubMed: 12894212]

DuBois RN, McLane MW, Ryder K, Lau LF, Nathans D. A growth factor-inducible nuclear protein with a novel cysteine/histidine repetitive sequence. J Biol Chem. 1990; 265:19185–19191. [PubMed: 1699942]

Fabian MR, Frank F, Rouya C, Siddiqui N, Lai WS, Karetnikov A, Blackshear PJ, Nagar B, Sonenberg N. Structural basis for the recruitment of the human CCR4-NOT deadenylase complex by tristetraprolin. Nat Struct Mol Biol. 2013; 20:735–739. [PubMed: 23644599]

Farley BM, Pagano JM, Ryder SP. RNA target specificity of the embryonic cell fate determinant POS-1. RNA. 2008; 14:2685–2697. [PubMed: 18952820]

Garneau NL, Wilusz J, Wilusz CJ. The highways and byways of mRNA decay. Nat Rev Mol Cell Biol. 2007; 8:113–126. [PubMed: 17245413]

Guan KL, Dixon JE. Eukaryotic proteins expressed in Escherichia coli: an improved thrombin cleavage and purification procedure of fusion proteins with glutathione S-transferase. Anal Biochem. 1991; 192:262–267. [PubMed: 1852137]

Gutierrez RA, Ewing RM, Cherry JM, Green PJ. Identification of unstable transcripts in Arabidopsis by cDNA microarray analysis: rapid decay is associated with a group of touch- and specific clock-controlled genes. Proc Natl Acad Sci U S A. 2002; 99:11513–11518. [PubMed: 12167669]

Heximer SP, Forsdyke DR. A human putative lymphocyte G0/G1 switch gene homologous to a rodent gene encoding a zinc-binding potential transcription factor. DNA Cell Biol. 1993; 12:73–88. [PubMed: 8422274]

Heyduk T, Ma Y, Tang H, Ebright RH. Fluorescence anisotropy: rapid, quantitative assay for protein-DNA and protein-protein interaction. Methods Enzymol. 1996; 274:492–503. [PubMed: 8902827]

Hudson BP, Martinez-Yamout MA, Dyson HJ, Wright PE. Recognition of the mRNA AU-rich element by the zinc finger domain of TIS11d. Nat Struct Mol Biol. 2004; 11:257–264. [PubMed: 14981510]

Jan A, Maruyama K, Todaka D, Kidokoro S, Abo M, Yoshimura E, Shinozaki K, Nakashima K, Yamaguchi-Shinozaki K. OsTZF1, a CCCH-tandem zinc finger protein, confers delayed senescence and stress tolerance in rice by regulating stress-related genes. Plant Physiol. 2013

Jang JC, Fujioka S, Tasaka M, Seto H, Takatsuto S, Ishii A, Aida M, Yoshida S, Sheen J. A critical role of sterols in embryonic patterning and meristem programming revealed by the fackel mutants of Arabidopsis thaliana. Genes Dev. 2000; 14:1485–1497. [PubMed: 10859167]

Jenkins TH, Li J, Scutt CP, Gilmartin PM. Analysis of members of the Silene latifolia Cys2/His2 zinc-finger transcription factor family during dioecious flower development and in a novel stamen-defective mutant ssf1. Planta. 2005; 220:559–571. [PubMed: 15703927]

Kim DH, Yamaguchi S, Lim S, Oh E, Park J, Hanada A, Kamiya Y, Choi G. SOMNUS, a CCCH-type zinc finger protein in Arabidopsis, negatively regulates light-dependent seed germination downstream of PIL5. Plant Cell. 2008; 20:1260–1277. [PubMed: 18487351]

Kim J, Somers DE. Rapid assessment of gene function in the circadian clock using artificial microRNA in Arabidopsis mesophyll protoplasts. Plant Physiol. 2010; 154:611–621. [PubMed: 20709829]

Klug A, Schwabe JW. Protein motifs 5. Zinc fingers. FASEB J. 1995; 9:597–604. [PubMed: 7768350]

Kong Z, Li M, Yang W, Xu W, Xue Y. A novel nuclear-localized CCCH-type zinc finger protein, OsDOS, is involved in delaying leaf senescence in rice. Plant Physiol. 2006; 141:1376–1388. [PubMed: 16778011]

Kruger, NJ. The Bradford Method for Protein Quantification. In: Walker, JM., editor. The Protein Protocols Handbook. 2nd Edition. Humana Press Inc.; Totowa: 2002.

Lai WS, Blackshear PJ. Interactions of CCCH zinc finger proteins with mRNA: tristetraprolin-mediated AU-rich element-dependent mRNA degradation can occur in the absence of a poly(A) tail. J Biol Chem. 2001; 276:23144–23154. [PubMed: 11279239]

Lai WS, Carballo E, Strum JR, Kennington EA, Phillips RS, Blackshear PJ. Evidence that tristetraprolin binds to AU-rich elements and promotes the deadenylation and destabilization of tumor necrosis factor alpha mRNA. Mol Cell Biol. 1999; 19:4311–4323. [PubMed: 10330172]

Lai WS, Carballo E, Thorn JM, Kennington EA, Blackshear PJ. Interactions of CCCH zinc finger proteins with mRNA. Binding of tristetraprolin-related zinc finger proteins to Au-rich elements and destabilization of mRNA. J Biol Chem. 2000; 275:17827–17837. [PubMed: 10751406]

Lai WS, Kennington EA, Blackshear PJ. Interactions of CCCH zinc finger proteins with mRNA: non-binding tristetraprolin mutants exert an inhibitory effect on degradation of AU-rich element-containing mRNAs. J Biol Chem. 2002; 277:9606–9613. [PubMed: 11782475]

Lai WS, Perera L, Hicks SN, Blackshear PJ. Mutational and structural analysis of the tandem zinc finger domain of tristetraprolin. J Biol Chem. 2013

Lai WS, Stumpo DJ, Blackshear PJ. Rapid insulin-stimulated accumulation of an mRNA encoding a proline-rich protein. J Biol Chem. 1990; 265:16556–16563. [PubMed: 2204625]

Laity JH, Lee BM, Wright PE. Zinc finger proteins: new insights into structural and functional diversity. Curr Opin Struct Biol. 2001; 11:39–46. [PubMed: 11179890]

Lee SJ, Jung HJ, Kang H, Kim SY. Arabidopsis zinc finger proteins AtC3H49/AtTZF3 and AtC3H20/AtTZF2 are involved in ABA and JA responses. Plant Cell Physiol. 2012; 53:673–686. [PubMed: 22383628]

Li Z, Thomas TL. PEI1, an embryo-specific zinc finger protein gene required for heart-stage embryo formation in Arabidopsis. Plant Cell. 1998; 10:383–398. [PubMed: 9501112]

Licatalosi DD, Darnell RB. RNA processing and its regulation: global insights into biological networks. Nat Rev Genet. 2010; 11:75–87. [PubMed: 20019688]

Lin PC, Pomeranz MC, Jikumaru Y, Kang SG, Hah C, Fujioka S, Kamiya Y, Jang JC. The Arabidopsis tandem zinc finger protein AtTZF1 affects ABA- and GA-mediated growth, stress and gene expression responses. Plant J. 2011; 65:253–268. [PubMed: 21223390]

Livak KJ, Schmittgen TD. Analysis of relative gene expression data using real-time quantitative PCR and the 2(-Delta Delta C(T)) Method. Methods. 2001; 25:402–408. [PubMed: 11846609]

Lunde BM, Moore C, Varani G. RNA-binding proteins: modular design for efficient function. Nat Rev Mol Cell Biol. 2007; 8:479–490. [PubMed: 17473849]

Ma Q, Herschman HR. A corrected sequence for the predicted protein from the mitogen-inducible TIS11 primary response gene. Oncogene. 1991; 6:1277–1278. [PubMed: 1861870]

Martin KC, Ephrussi A. mRNA localization: gene expression in the spatial dimension. Cell. 2009; 136:719–730. [PubMed: 19239891]

Mathieu O, Yukawa Y, Prieto JL, Vaillant I, Sugiura M, Tourmente S. Identification and characterization of transcription factor IIIA and ribosomal protein L5 from Arabidopsis thaliana. Nucleic Acids Res. 2003; 31:2424–2433. [PubMed: 12711688]

Moore M, Ullman C. Recent developments in the engineering of zinc finger proteins. Brief Funct Genomic Proteomic. 2003; 1:342–355. [PubMed: 15239882]

Muench DG, Zhang C, Dahodwala M. Control of cytoplasmic translation in plants. Wiley Interdiscip Rev RNA. 2012; 3:178–194. [PubMed: 22215505]

Narsai R, Howell KA, Millar AH, O'Toole N, Small I, Whelan J. Genome-wide analysis of mRNA decay rates and their determinants in Arabidopsis thaliana. Plant Cell. 2007; 19:3418–3436. [PubMed: 18024567]

Pagano JM, Farley BM, McCoig LM, Ryder SP. Molecular basis of RNA recognition by the embryonic polarity determinant MEX-5. J Biol Chem. 2007; 282:8883–8894. [PubMed: 17264081]

Pedro-Segura E, Vergara SV, Rodriguez-Navarro S, Parker R, Thiele DJ, Puig S. The Cth2 ARE-binding protein recruits the Dhh1 helicase to promote the decay of succinate dehydrogenase SDH4 mRNA in response to iron deficiency. J Biol Chem. 2008; 283:28527–28535. [PubMed: 18715869]

Pomeranz M, Finer J, Jang JC. Putative molecular mechanisms underlying tandem CCCH zinc finger protein mediated plant growth, stress, and gene expression responses. Plant Signal Behav. 2011a; 6:647–651. [PubMed: 21795857]

Pomeranz M, Zhang L, Finer J, Jang JC. Can AtTZF1 act as a transcriptional activator or repressor in plants? Plant Signal Behav. 2011b; 6:719–722. [PubMed: 21455027]

Pomeranz MC, Hah C, Lin PC, Kang SG, Finer JJ, Blackshear PJ, Jang JC. The Arabidopsis tandem zinc finger protein AtTZF1 traffics between the nucleus and cytoplasmic foci and binds both DNA and RNA. Plant Physiol. 2010; 152:151–165. [PubMed: 19897605]

Puig S, Askeland E, Thiele DJ. Coordinated remodeling of cellular metabolism during iron deficiency through targeted mRNA degradation. Cell. 2005; 120:99–110. [PubMed: 15652485]

Puig S, Vergara SV, Thiele DJ. Cooperation of two mRNA-binding proteins drives metabolic adaptation to iron deficiency. Cell Metab. 2008; 7:555–564. [PubMed: 18522836]

Raghavan A, Robison RL, McNabb J, Miller CR, Williams DA, Bohjanen PR. HuA and tristetraprolin are induced following T cell activation and display distinct but overlapping RNA binding specificities. J Biol Chem. 2001; 276:47958–47965. [PubMed: 11602610]

Ross J. mRNA stability in mammalian cells. Microbiol Rev. 1995; 59:423–450. [PubMed: 7565413]

Schmalzbauer E, Strack B, Dannull J, Guehmann S, Moelling K. Mutations of basic amino acids of NCp7 of human immunodeficiency virus type 1 affect RNA binding in vitro. J Virol. 1996; 70:771–777. [PubMed: 8551614]

Schubert CM, Lin R, de Vries CJ, Plasterk RH, Priess JR. MEX-5 and MEX-6 function to establish soma/germline asymmetry in early C. elegans embryos. Mol Cell. 2000; 5:671–682. [PubMed: 10882103]

Schumann U, Prestele J, O'Geen H, Brueggeman R, Wanner G, Gietl C. Requirement of the C3HC4 zinc RING finger of the Arabidopsis PEX10 for photorespiration and leaf peroxisome contact with chloroplasts. Proc Natl Acad Sci U S A. 2007; 104:1069–1074. [PubMed: 17215364]

Sheen J. Signal transduction in maize and Arabidopsis mesophyll protoplasts. Plant Physiol. 2001; 127:1466–1475. [PubMed: 11743090]

Stewart-Maynard KM, Cruceanu M, Wang F, Vo MN, Gorelick RJ, Williams MC, Rouzina I, Musier-Forsyth K. Retroviral nucleocapsid proteins display nonequivalent levels of nucleic acid chaperone activity. J Virol. 2008; 82:10129–10142. [PubMed: 18684831]

Sun J, Jiang H, Xu Y, Li H, Wu X, Xie Q, Li C. The CCCH-type zinc finger proteins AtSZF1 and AtSZF2 regulate salt stress responses in Arabidopsis. Plant Cell Physiol. 2007; 48:1148–1158. [PubMed: 17609218]

Takatsuji H. Zinc-finger transcription factors in plants. Cell Mol Life Sci. 1998; 54:582–596. [PubMed: 9676577]

Tam PP, Barrette-Ng IH, Simon DM, Tam MW, Ang AL, Muench DG. The Puf family of RNA-binding proteins in plants: phylogeny, structural modeling, activity and subcellular localization. BMC Plant Biol. 2010; 10:44. [PubMed: 20214804]

Vargas DY, Raj A, Marras SA, Kramer FR, Tyagi S. Mechanism of mRNA transport in the nucleus. Proc Natl Acad Sci U S A. 2005; 102:17008–17013. [PubMed: 16284251]

Vergara SV, Puig S, Thiele DJ. Early recruitment of AU-rich element-containing mRNAs determines their cytosolic fate during iron deficiency. Mol Cell Biol. 2011; 31:417–429. [PubMed: 21135132]

Walia RR, Caragea C, Lewis BA, Towfic F, Terribilini M, El-Manzalawy Y, Dobbs D, Honavar V. Protein-RNA interface residue prediction using machine learning: an assessment of the state of the art. BMC Bioinformatics. 2012; 13:89. [PubMed: 22574904]

Wang D, Guo Y, Wu C, Yang G, Li Y, Zheng C. Genome-wide analysis of CCCH zinc finger family in Arabidopsis and rice. BMC Genomics. 2008; 9:44. [PubMed: 18221561]

Wang L, Brown SJ. BindN: a web-based tool for efficient prediction of DNA and RNA binding sites in amino acid sequences. Nucleic Acids Res. 2006; 34:W243–248. [PubMed: 16845003]

Wells DG. mRNA translation: regulating an out of soma experience. Curr Opin Cell Biol. 2012; 24:554–557. [PubMed: 22770873]

Westermeier R. Sensitive, quantitative, and fast modifications for Coomassie Blue staining of polyacrylamide gels. Proteomics. 2006; 6(Suppl 2):61–64. [PubMed: 17031800]

Worthington MT, Amann BT, Nathans D, Berg JM. Metal binding properties and secondary structure of the zinc-binding domain of Nup475. Proc Natl Acad Sci U S A. 1996; 93:13754–13759. [PubMed: 8943007]

Worthington MT, Pelo JW, Sachedina MA, Applegate JL, Arseneau KO, Pizarro TT. RNA binding properties of the AU-rich element-binding recombinant Nup475/TIS11/tristetraprolin protein. J Biol Chem. 2002; 277:48558–48564. [PubMed: 12324455]

Zhang C, Zhang F, Zhou J, Fan Z, Chen F, Ma H, Xie X. Overexpression of a phytochrome-regulated tandem zinc finger protein gene, OsTZF1, confers hypersensitivity to ABA and hyposensitivity to red light and far-red light in rice seedlings. Plant Cell Rep. 2012; 31:1333–1343. [PubMed: 22572927]

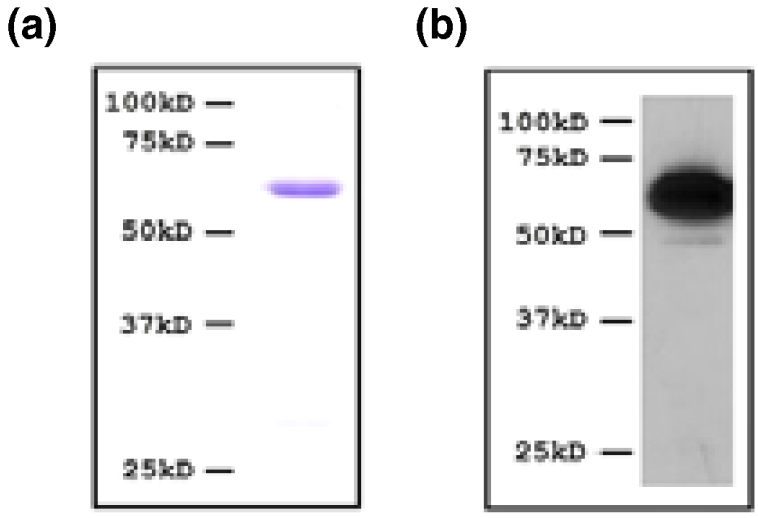

Figure 1.

Recombinant full-length GST-AtTZF1 proteins. (a) Coomassie blue staining of GST-AtTZF1. (b) Identification of GST-AtTZF1 by western blot analysis using anti-AtTZF1 antibodies. The molecular weight of GST-AtTZF1 is 61.4 kD.

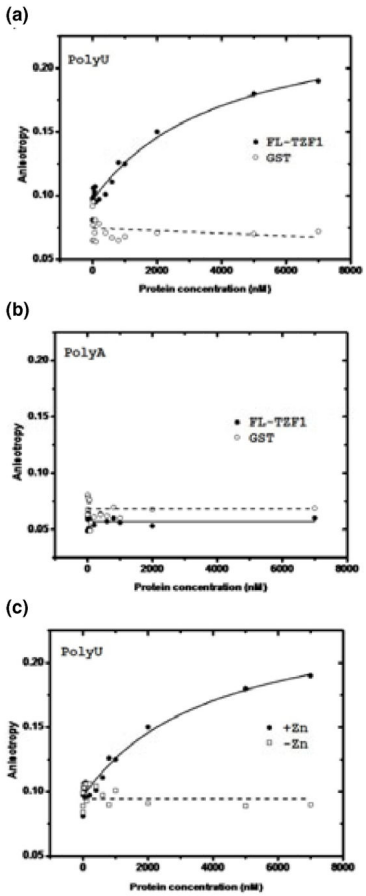

Figure 2.

Full-length GST-AtTZF1 binds to specific RNA molecules in a zinc-dependent manner. Full-length GST-AtTZF1 binds to polyU (a) but not to polyA (b) in fluorescence anisotropy (FA) analysis. Binding specificity is supported by negative results using GST alone. (c) AtTZF1 binding to polyU is dependent on the presence of zinc.

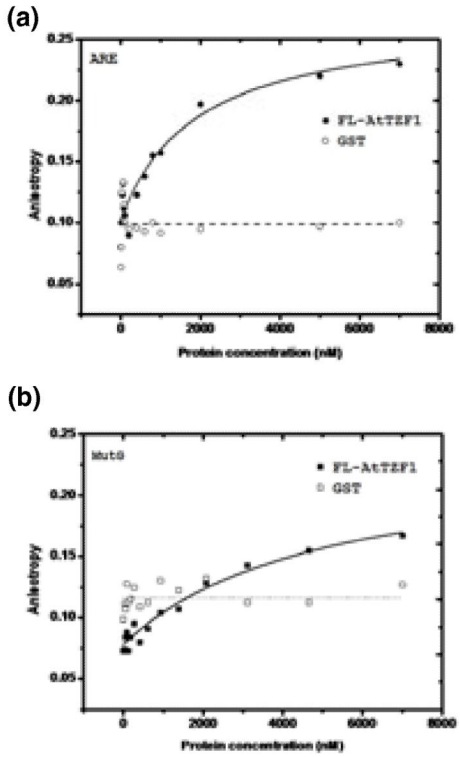

Figure 3.
Full-length GST-AtTZF1 binds to ARE_{19} (a) with stronger affinity than to MutG (b) in FA analysis. GST is used as a negative control in both experiments.

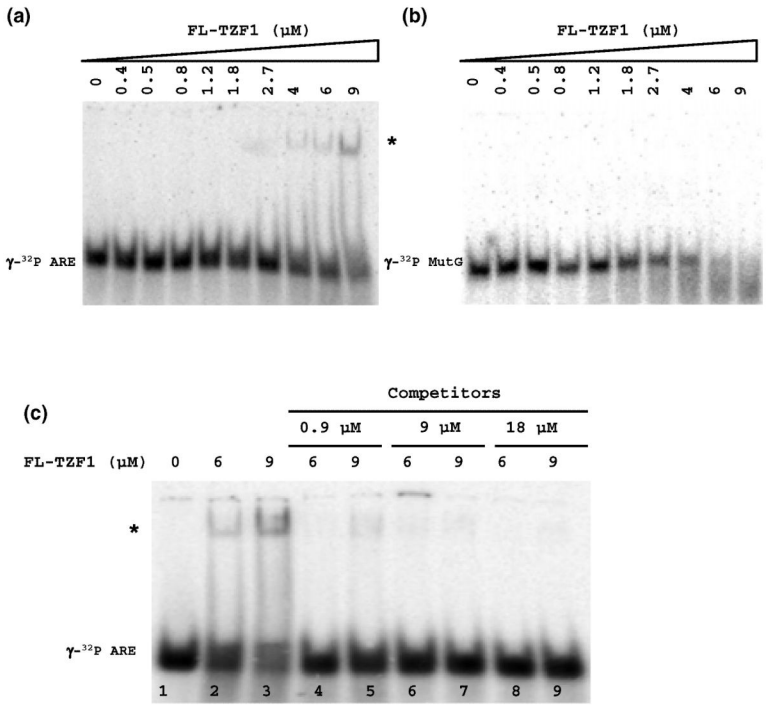

Figure 4.

Full-length GST-AtTZF1 interacts with ARE_{19} in RNA electrophoretic mobility shift assays (EMSA). (a) AtTZF1 binds to ^{32}P-labeled ARE_{19}. (b) AtTZF1 does not bind to MutG. (c) Labeled RNA-protein complexes can be eliminated by the competition of unlabeled ARE_{19} (lane 4-9). RNA-protein complexes are indicated by asterisk.

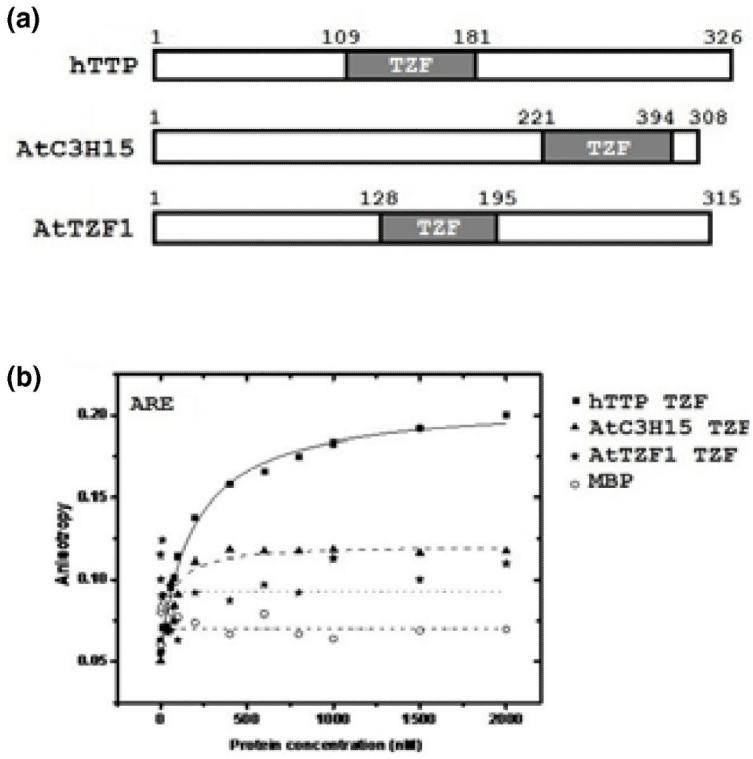

Figure 5.

Comparison of RNA binding affinity among different TZF domains from hTTP, AtC3H15, and AtTZF1. (a) Schematic representation of TZF motifs in gray bars. (b) Interactions between various TZF domains and ARE_{19} in FA analysis. Binding specificity is supported by negative results using MBP alone.

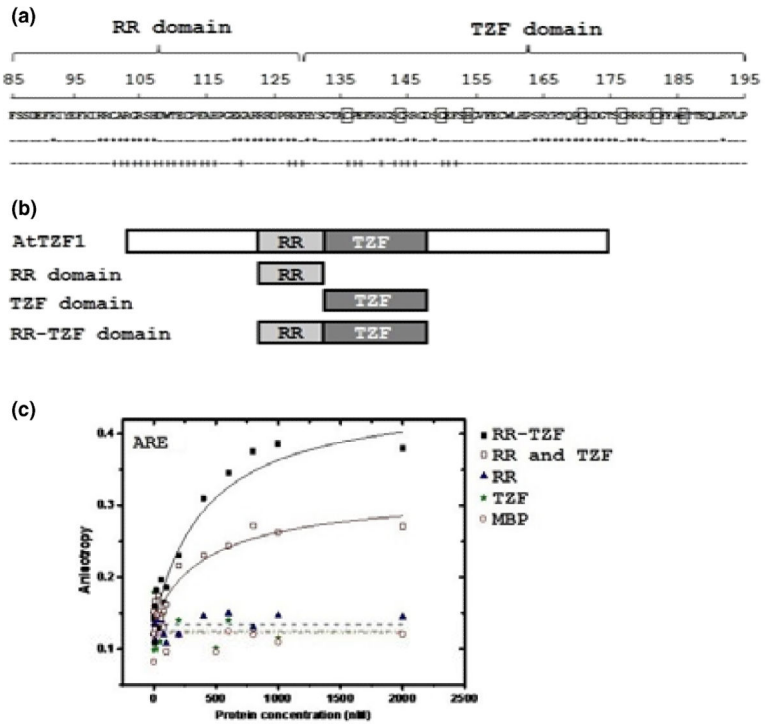

Figure 6.

Analysis of AtTZF1 RR-TZF domain in RNA binding potential. (a) Prediction of RNA-interacting residues in AtTZF1 RR-TZF region (amino acid 85-195) using BindN (http://bioinfo.ggc.org/bindn/) and RNABindR (http://einstein.cs.iastate.edu/RNABindRPlus/) program, respectively. * and + indicate RNA-binding residues predicted by BindN and RNABindR, respectively. (b) Schematic representation of AtTZF1 domain constructs used in this study. (c) The RR-TZF, but not the RR or TZF domain alone, of AtTZF1 binds to ARE_{19}. RR and TZF (empty square symbol) represents a 1:1 mixture of the RR and TZF domains. Binding specificity is supported by negative results using MBP alone.

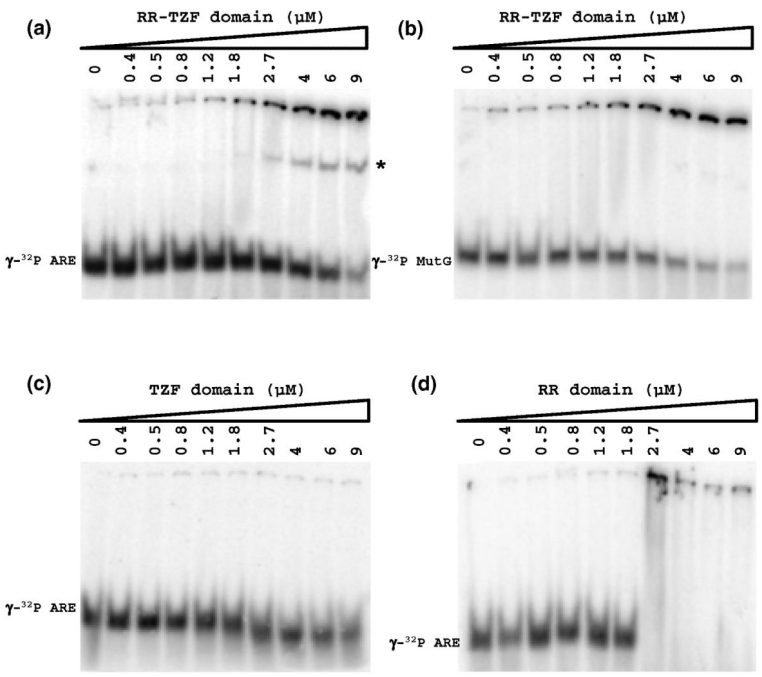

Figure 7.

EMSA results of truncated AtTZF1 proteins with ^{32}P-labeled oligoribonucleotide probes. RR-TZF domain binds to ARE_{19} (a), but not to MutG (b). Neither TZF (c) nor RR (d) domain binds to ARE_{19}. RNA-protein complexes are indicated by asterisk.

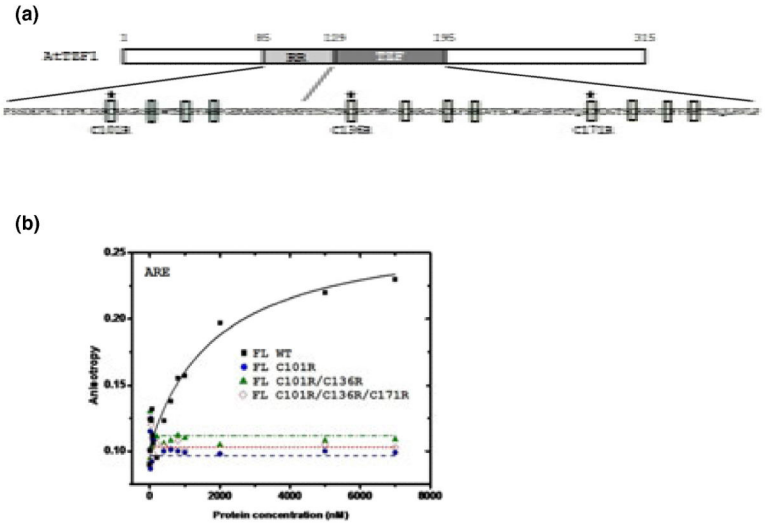

Figure 8.

The effects of point mutations in the RR-TZF domain on AtTZF1-RNA interaction. (a) Schematic representation of site-directed mutations in the RR-TZF domain of AtTZF1. (b) The effects of point mutations on full-length AtTZF1 (FL) binding to fluorescein-labeled ARE_{19} in FA analyses.

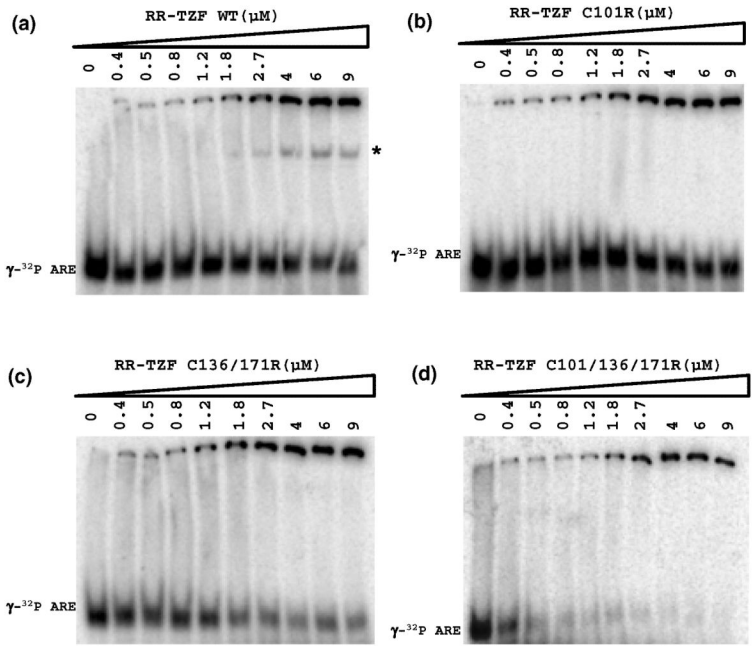

Figure 9.

The effects of point mutations on RR-TZF binding to ^{32}P-labeled ARE_{19} in EMSAs. (a) wild-type RR-TZF domain. (b) RR-TZF C101R mutant. (c) RR-TZF C101R/C136R mutant. (d) RR-TZF C101R/C136R/C171R mutant. RNA-protein complexes are indicated by asterisk.

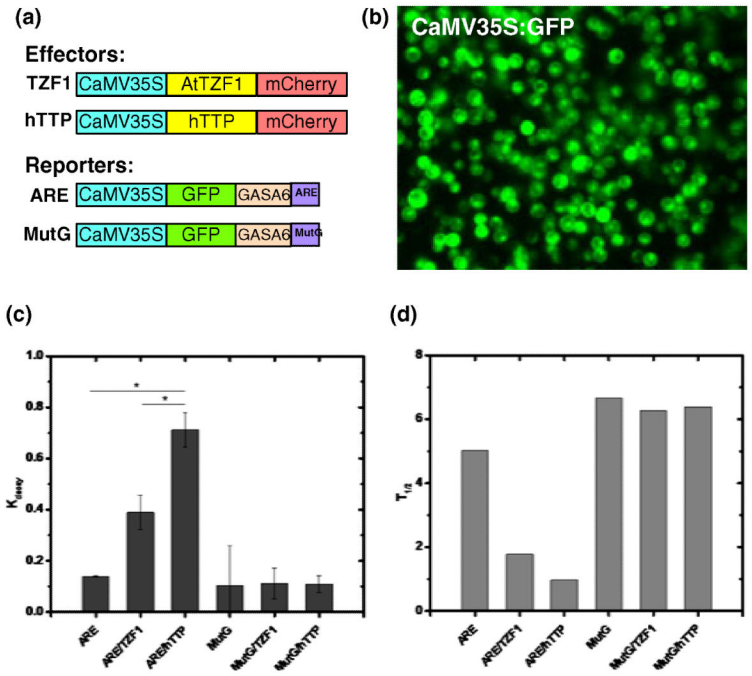

Figure 10.

Determine the effects of AtTZF1 and hTTP on mRNA stability using a maize protoplast transient expression system. (a) Effectors and reporters used in this analysis. (b) High efficiency protoplast transformation is shown by the expression of free GFP. Decay rates (c) and half-lives (d) of reporter genes under the influence of different effectors. Significant differences are indicated by asterisks (*P < 0.05). ARE: TTATTTATTATTTATTTATTATTTATTTATTATTTATTTATTA(28) MutG:TTGTTTGTTGTTTGTTTGTTGTTTGTTTGTTGTTTGTTTGTTA(28)

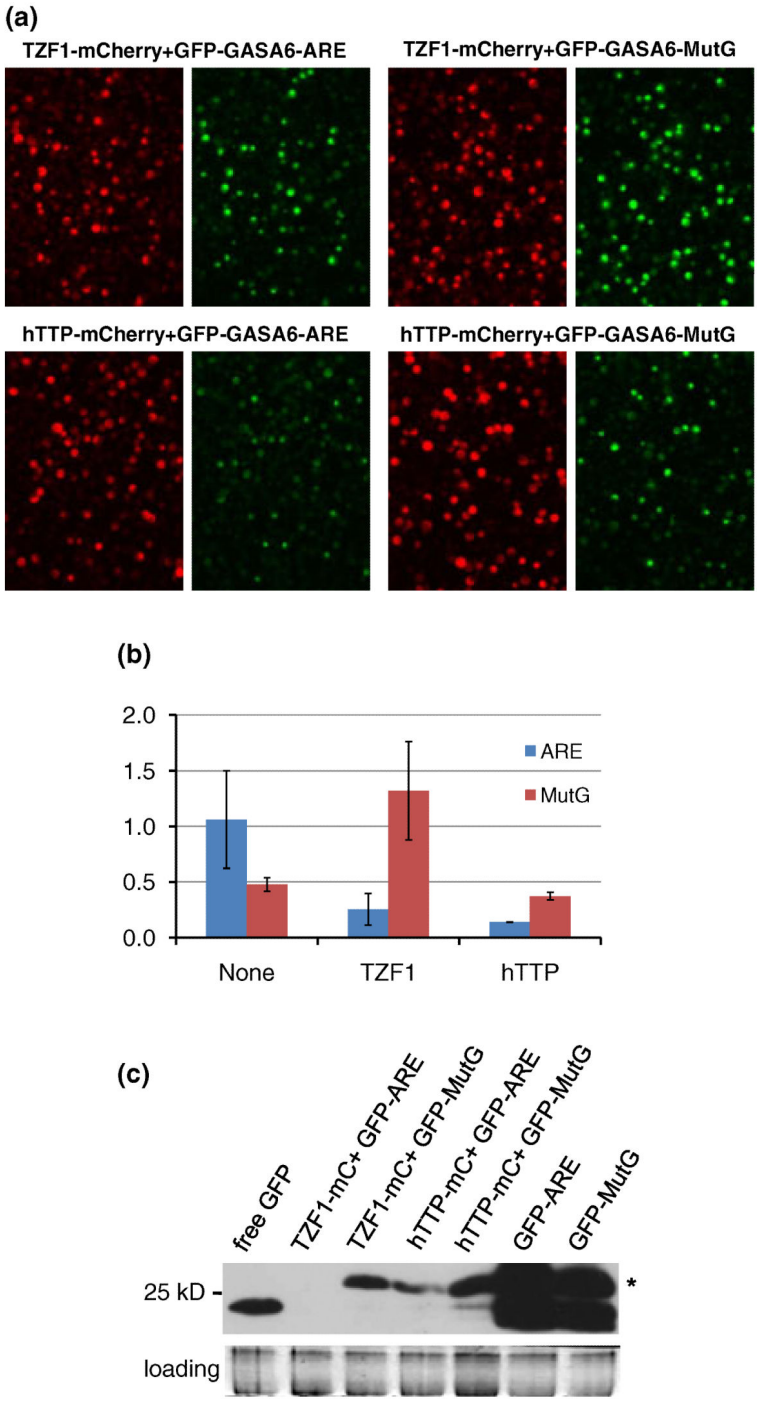

Figure 11.

The effects of AtTZF1 and hTTP on ARE-containing mRNA accumulation in maize protoplast transient expression analyses. (a) Shown are protoplasts expressing fusion proteins from 4 independent samples co-transformed with a distinct pair of effector and reporter. Transformed protoplasts were incubated in the dark at 25°C for 14 h in the absence of Actinomycin D. Each pair of images was taken from the same population of protoplasts under fluorescence microscope using two different filters to reveal GFP and mCherry

expression, respectively. (b) The effects of AtTZF1 and hTTP on the expression of reporter genes (GFP-ARE and GFP-MutG). Relative expression was normalized by PP2A expression using qRT-PCR analysis. (c) Reporter protein accumulation was quantified by Western blot analysis using α-GFP. Fusion proteins are indicated by asterisk.

Table 1

RNA probes used in this study

Probe	Sequence (5′ to 3′)
Fl-polyU	Fl-UUUUUUUUUUUUUUUUUUU
Fl-polyA	Fl-AAAAAAAAAAAAAAAAAAA
Fl-ARE_{13}	Fl-AUUUAUUUAUUUA
Fl-ARE_{19}	Fl-UAUUUAUUAUUUAUUUAUU
Fl-MutG	Fl-UGUUUGUUGUUUGUUUGUU
ARE_{19}	UAUUUAUUAUUUAUUUAUU
MutG	UGUUUGUUGUUUGUUUGUU

“Fl” indicates the positions of the 6-carboxyfluorescein moieties conjugated to applicable RNA substrates.

Table 2

FA analysis of full-length GST-AtTZF1 (WT and point mutations) binding to RNAs

RNA probe	K_d (nM) at 25°C				
	WT	**C101R**	**C136R/C171R**	**C101R/C136R/C171R**	**GST**
Fl-polyU	2270±190	$>10^4$	$>10^4$	$>10^4$	$>10^4$
Fl-polyA	$>10^4$	ND[a]	ND	ND	$>10^4$
Fl-ARE_{19}	4550±130	$>10^4$	$>10^4$	$>10^4$	$>10^4$
Fl-ARE_{13}	$>10^4$	ND	ND	ND	$>10^4$
Fl-MutG	8740±380	ND	ND	ND	$>10^4$

Equilibrium binding constants are calculated by fitting the data from FA experiments by non-linear regression using Equation 1. The value of K_d is represented by mean±standard deviation from 2 or 3 experimental replicates.

[a]ND, not determined.

Table 3

Analysis of the TZF and RR-TZF domains binding to RNAs

	K_d (nM) at 25°C			
MBP fusion proteins	**Fl-polyU**	**Fl-ARE$_{19}$**	**Fl-ARE$_{13}$**	**Fl-MutG**
hTTP TZF	2290±100	340±40	200±30	$>10^4$
AtC3H15 TZF	$>10^4$	130 ±20	ND[a]	ND
AtTZFl TZF	7370±120	$>10^4$	ND	ND
AtTZF1 RR	$>10^4$	$>10^4$	ND	ND
AtTZF1 RR-TZF	470±30	410±50	ND	ND
AtTZF1 RR and AtTZF1 TZF	4400±100	610±40	ND	ND
AtTZF1 RR-TZF C101R	810±40	740±40	ND	ND
AtTZF1 RR-TZF C136R/C171R	1610±40	1540±50	ND	ND
AtTZF1 RR-TZF C101R/C136R/C171R	3110±80	3030±80	ND	ND
Control (MBP)	$>10^4$	$>10^4$	$>10^4$	$>10^4$

Equilibrium binding constants are calculated from binding curves that have been described using non-linear regression (Equation 1). The value of K_d is represented by mean±standard deviation from 2 or 3 experimental replicates.

[a] ND, not determined.

Table 4

The effects of zinc on TZF protein-RNA interaction

Proteins	K_d (nM) at 25°C			
	Fl-polyU		Fl-ARE_{19}	
	Zn(+)	Zn(−)	Zn(+)	Zn(−)
Full-length AtTZFl	2270±190	>104	4550±130	>104
AtTZFl RR-TZF	470±30	3200±40	410±30	2910 ± 50
AtC3H15 TZF	>104	>104	130±20	>104

Equilibrium binding constants are calculated from binding curves resolved by non-linear regression using Equation 1. The value of K_d is represented by mean±σ for 2-3 experimental replicates.